

## Flow equations in generalized braneworld scenarios

Gianluca Calcagni,<sup>1</sup> Andrew R. Liddle,<sup>2</sup> and Erandy Ramírez<sup>2</sup>

<sup>1</sup>*Department of Physics, Gunma National College of Technology, Gunma 371-8530, Japan*

<sup>2</sup>*Astronomy Centre, University of Sussex, Brighton BN1 9QH, United Kingdom*

(Dated: June 23rd, 2005)

We discuss the flow equations in the context of general braneworld cosmologies with a modified Friedmann equation, for either an ordinary scalar field or a Dirac–Born–Infeld tachyon as inflaton candidates. The 4D, Randall–Sundrum, and Gauss–Bonnet cases are compared, using the patch formalism which provides a unified description of these models. The inflationary dynamics is described by a tower of flow parameters that can be evolved in time to select a particular subset of points in the space of cosmological observables. We analyze the stability of the fixed points in all the cosmologies (our results in the 4D case already extending those in the literature). Numerical integration of the flow equations shows that the predictions of the Gauss–Bonnet braneworld differ significantly as compared to the Randall–Sundrum and 4D scenarios, whereas tachyon inflation gives tensor perturbations smaller than those in the presence of a normal scalar field. These results are extended to the realization of a noncommutative space-time preserving maximal symmetry. In this case the tensor-to-scalar signal is unchanged, while blue-tilted spectra are favoured.

PACS numbers: 98.80.Cq, 04.50.+h

### I. INTRODUCTION

The recent improvement in the determination of cosmological observables by the Wilkinson Microwave Anisotropy Probe [1, 2] and other large-scale structure experiments has given a boost to the search for viable theoretical scenarios of the early Universe. An important problem cosmologists still have to address is cosmic confusion in inflationary scenarios, whereby different underlying physics leads to the same observables; deriving robust conclusions from data requires an understanding of such model degeneracies. Viable inflation models must predict the quasi-invariant density perturbation spectra and subdominant tensor perturbations that observations require, but having done so it is then difficult to discriminate between different details such as the precise shape of the potential. Indeed, even quite radical revisions of understanding of high-energy physics, such as the braneworld scenario, have yet to lead to appreciably characteristic predictions, at least in the simplest cases (see Ref. [3] for some reviews).

Rather than choosing a particular class of potentials and calculating the preferred values in the parameter space, one can try to circumscribe the allowed regions within it through the general behaviour of the inflationary dynamics. This can be achieved, for instance, by the study of the consistency equations, which do not depend on the choice of the potential; see Ref. [4] and references therein. Another possibility is to consider the evolution of the so-called flow parameters in terms of the number of  $e$ -foldings [5, 6, 7]. The flow equations naturally select a subset in the observational plane defined by the scalar spectral index  $n_s$  and the tensor-to-scalar ratio  $r$ . Modifications to the underlying dynamics will lead to a shift in the location of that subset, helping to indicate whether a particular class of inflationary models is better able to produce observables in the region required by data.

In this paper we shall explore the flow approach in several braneworld scenarios, where the effective Friedmann equation governing the cosmological brane dynamics is modified with respect to the 4D evolution. The simplest such case, the Randall–Sundrum (RS) type II model for a normal scalar field, was already considered in Ref. [8] and found not to introduce qualitatively different features. Here we shall extend the discussion to the Gauss–Bonnet (GB) braneworld by means of the “patch formalism” [4], which provides a unified description of a wide range of possible gravity models. This has the advantage that we can simultaneously implement general inflationary scenarios with modified Friedmann equations and either an ordinary or Dirac–Born–Infeld (DBI) tachyonic scalar field. The goal is to seek new insights into the general structure of braneworld and tachyon scenarios via a technique that might give complementary information as compared to model-building approaches.

We will find that in the Gauss–Bonnet case with normal scalar field, the flow structure in the  $n_s$ – $r$  plane is quite different from the 4D and RS cases because of the details of the flow equations. The flow structure for the tachyon models, here presented for the first time, gives independent support to other results found in literature; in particular, the most characteristic prediction is the generation of spectra with a rather low tensor-to-scalar ratio. The stability of the fixed points in the plane is also analyzed at higher order in the flow parameters.

Finally, we shall consider how the general relativistic and braneworld scenarios are affected by the introduction of a noncommutative space-time algebra, which modifies the inflationary anisotropies while leaving the homogeneous background (and the associated flow equations) untouched [9]. This skews the theoretical points in the  $n_s$ – $r$  plane towards the blue-tilted region, with models having a high tensor-to-scalar ratio suffering the largest shifts.

## II. FORMALISM

### A. The patch universe

We shall assume that the universe is confined into a 3-brane embedded in a five-dimensional bulk. Matter lives on the brane only, while gravitons are free to propagate in the bulk. This is guaranteed as long as the effective energy density measured by the observer is smaller than the mass scale of the theory,  $\rho < m_5^4$ . By restricting our attention to the inflationary physics, we can disregard the contribution of the projected Weyl tensor at large scales.

If the energy density on the brane is comparable to the potential energy adopted to stabilize the extra dimension, the bulk backreacts and the effective cosmological evolution is modified by nonstandard terms. In particular, we can describe the primordial universe, at least in some finite time interval or energy patch, by the Friedmann equation

$$H^2 = \beta_q^2 \rho^q, \quad (1)$$

where  $q$  is constant and  $\beta_q > 0$  is a constant factor with energy dimension  $[\beta_q] = E^{1-2q}$ . This equation encodes a number of situations, including the pure 4D radion-stabilized regime ( $q = 1$ , also known as the standard cosmology), the high-energy limit of the Randall–Sundrum braneworld ( $q = 2$ ), and the high-energy limit of the Gauss–Bonnet scenario ( $q = 2/3$ ). Defining the parameter

$$\theta \equiv 2(1 - q^{-1}), \quad (2)$$

Eq. (1) can be recast as

$$H^{2-\theta} = \beta_q^{2-\theta} \rho. \quad (3)$$

Deviations from the 4D case  $\theta = 0$  will characterize exotic scenarios (braneworlds or modified gravities) according to their magnitude and sign.

Because of local conservation of the energy–momentum tensor, for a perfect fluid with pressure  $p$  the continuity equation is

$$\dot{\rho} + 3H(\rho + p) = 0. \quad (4)$$

The dynamics of the patch inflationary universe has been extensively explored in the case of both an ordinary scalar inflaton  $\phi$  and a DBI tachyon  $T$ ; for a complete review of results and a list of references see Ref. [4]. It is useful to generically label the inflaton field as  $\psi$  and introduce a new parameter

$$\tilde{\theta} = \theta \quad \text{for } \psi = \phi, \quad (5a)$$

$$\tilde{\theta} = 2 \quad \text{for } \psi = T. \quad (5b)$$

Let  $H_0$  be the Hubble parameter evaluated at some reference time  $t_0$  (later it will correspond to the integration

starting time). The quantity

$$\alpha_q \equiv \frac{1}{\beta_q} \sqrt{\frac{2}{3q} \left( \frac{\beta_q}{H_0} \right)^{\tilde{\theta}}}, \quad (6)$$

has dimension  $[\alpha_q] = E^{q(2-\tilde{\theta})-1}$  ( $= E^{-1}$  for  $\psi = T$  and  $= E$  for  $\psi = \phi$ ), and can be absorbed in the normalization of the scalar field, so that the latter becomes dimensionless. In the following we use the redefinition  $\psi \rightarrow \psi/\alpha_q$  everywhere; all dropped  $\alpha_q$  factors can be recovered by counting the number of  $\psi$  derivatives.

### B. Slow-roll parameters and flow equations

The amount of inflation is described by the number of  $e$ -foldings

$$N(t) \equiv \ln(a_f/a) = \int_t^{t_f} H(t') dt', \quad (7)$$

this “backward” definition measuring the number of remaining  $e$ -foldings at the time  $t$  before the end of inflation at  $t_f$ . In the flow approach, the cosmological variables during inflation are written as functions of  $N$  or  $\psi$ ; one can shift from one picture to the other via

$$\frac{d}{dN} = -\frac{d}{H dt} = \left( \frac{H_0}{H} \right)^{\tilde{\theta}} \frac{H'}{H} \frac{d}{d\psi}, \quad (8)$$

where a prime denotes differentiation with respect to  $\psi$ .

We define the flow parameters as

$$\begin{aligned} \lambda_0 &\equiv \epsilon \equiv \frac{d \ln H}{dN} \\ &= \left( \frac{H}{H_0} \right)^{\tilde{\theta}} \frac{\dot{\psi}^2}{H^2} = \left( \frac{H_0}{H} \right)^{\tilde{\theta}} \left( \frac{H'}{H} \right)^2, \end{aligned} \quad (9a)$$

$$\lambda_\ell \equiv \left( \frac{H_0}{H} \right)^{\tilde{\theta}\ell} \frac{H^{(\ell+1)} (H')^{\ell-1}}{H^\ell}, \quad \ell \geq 1. \quad (9b)$$

where  $(n)$  indicates the  $n$ -th  $\psi$  derivative. Usually in literature they are dubbed  ${}^\ell \lambda_H$ . Note that this definition can be obtained from the potential slow-roll (SR) tower of Ref. [4] with the substitutions  $\phi \rightarrow \psi$ ,  $V \rightarrow H$ , and  $q \rightarrow 1 + \tilde{\theta}$ . In four dimensions and with an ordinary scalar field this definition coincides with that of Ref. [6].

It is also convenient to consider the following quantity:

$$\sigma \equiv 2\lambda_1 - (4 + \theta + \tilde{\theta})\epsilon. \quad (10)$$

The set of evolution equations reads, from Eqs. (8), (9),

and (10),

$$\frac{d\epsilon}{dN} = \epsilon[\sigma + (2 + \theta)\epsilon], \quad (11a)$$

$$\frac{d\sigma}{dN} = 2\lambda_2 - (5 + 2\tilde{\theta} + \theta)\epsilon\sigma - (4 + \theta + \tilde{\theta})(3 + \theta + \tilde{\theta})\epsilon^2, \quad (11b)$$

$$\frac{d\lambda_\ell}{dN} = \lambda_{\ell+1} + \frac{1}{2}\lambda_\ell\{(\ell - 1)\sigma + [2\ell\tilde{\theta} - (4 + \theta + \tilde{\theta})]\epsilon\}, \quad \ell \geq 2, \quad (11c)$$

where  $2\tilde{\theta} \equiv 2 + \theta - \tilde{\theta}$ .

As shown in Ref. [7], the flow parameters and equations do not encode the inflationary dynamics, since they are only a set of identities for the Hubble rate  $H$  as a function of  $N$ . In fact, by definition the next-to-lowest-order SR terms appear with higher powers, and one can approximate the dynamics through a power truncation of the traditional SR tower. In the case of the flow parameters, Eq. (9), this is achieved by imposing a constraint such as  $H^{(\bar{n}+1)} = 0$  and  $H^{(\bar{n})} \neq 0$ , for some maximum  $\bar{n}$ . However, the method still provides an algorithm for generating inflationary models in the space of the cosmological observables, corresponding to a Taylor expansion of  $H(\psi)$  [7].

For reference, the flow parameters are related to the Hubble-slow-roll parameters, defined by [4, 10]

$$\epsilon_n \equiv \left(\frac{H_0}{H}\right)^{\tilde{\theta}} \frac{H'}{H} \left[\frac{H^{\tilde{\theta}}}{H'} \left(\frac{H'}{H^{\tilde{\theta}}}\right)^{(n)}\right]^{1/n}, \quad n \geq 1, \quad (12)$$

via the relation

$$\epsilon_n^n = \lambda_n \frac{H^{\tilde{\theta}}}{H^{(n+1)}} \left(\frac{H'}{H^{\tilde{\theta}}}\right)^{(n)}. \quad (13)$$

For a comparison between the two towers from an observational point of view, see Ref. [11].

### C. Attractors and observables

It is easy to find the attractors of the flow and project them on the  $\sigma$ - $\epsilon$  plane. One is the line corresponding to de Sitter (dS) fixed points

$$\epsilon^* = 0, \quad (14a)$$

$$\sigma^* = \text{const}, \quad (14b)$$

$$\lambda_\ell^* = 0, \quad \ell \geq 2, \quad (14c)$$

and the other is the power-law inflationary attractor

$$\epsilon^* = \text{const}, \quad (15a)$$

$$\sigma^* = -(2 + \theta)\epsilon, \quad (15b)$$

$$\lambda_2^* = \frac{1}{2}(1 + \tilde{\theta})(2 + \tilde{\theta})\epsilon^2, \quad (15c)$$

$$\lambda_{\ell+1}^* = \frac{1}{2} \left[ 2 + (1 + \ell)\tilde{\theta} \right] \lambda_\ell^* \epsilon^*, \quad \ell \geq 2. \quad (15d)$$

Note that the slope of the line Eq. (15b) depends on the braneworld model one is considering, but not on the type of scalar field on the brane.

To first-order in slow roll the cosmological observables are

$$r \approx \frac{\epsilon}{\zeta_q}, \quad n_s - 1 \approx \sigma, \quad (16)$$

where  $r \equiv A_t^2/A_s^2$  is the ratio between the tensor and scalar perturbation amplitudes and  $n_s$  is the scalar spectral index. The coefficient  $\zeta_q$  is equal to 1 in the 4D and GB cases [12], while  $\zeta_2 = 2/3$  in the RS scenario [13]. The expression for  $r$  is valid in all cases considered, while the expression for  $n_s$  is for the commutative geometry case only and will be modified later to address the noncommutative case.

The stability analysis of the above fixed points against linear perturbations in the flow parameters involves an infinite-dimensional parameter space. However, one can truncate the flow tower at  $\ell$ -th order and study the system order-by-order, seeking convergence of dynamical properties.

Define the vector  $X \equiv (\epsilon, \sigma, \lambda_2, \dots, \lambda_\ell)^t$ . The perturbation equation reads

$$\frac{d\delta X}{dN} = M\delta X, \quad (17)$$

where  $\delta X \equiv (\delta\epsilon, \delta\sigma, \dots)^t$  encodes the linear perturbations and  $M$  is a  $(\ell + 1) \times (\ell + 1)$  matrix whose elements  $m_{ij}$  ( $i, j = 0, \dots, \ell$ ) are evaluated at a fixed point. For  $i < 2$  (the first two rows) one has

$$m_{00} = 2(2 + \theta)\epsilon^*, \quad m_{01} = \epsilon^*, \quad (18a)$$

$$m_{10} = -[(5 + 2\tilde{\theta} + \theta)\sigma^* + 2(4 + \theta + \tilde{\theta})(3 + \theta + \tilde{\theta})\epsilon^*], \quad (18b)$$

$$m_{11} = -(5 + 2\tilde{\theta} + \theta)\epsilon^*, \quad m_{12} = 2, \quad (18c)$$

$$m_{ij} = 0, \quad j \geq i + 2, \quad (18d)$$

while for  $i \geq 2$

$$m_{i0} = \frac{1}{2}[2i\tilde{\theta} - (4 + \theta + \tilde{\theta})]\lambda_i^*, \quad (18e)$$

$$m_{i1} = \frac{1}{2}(i - 1)\lambda_i^*, \quad (18f)$$

$$m_{ii} = \frac{1}{2}\{(i - 1)\sigma^* + [2i\tilde{\theta} - (4 + \theta + \tilde{\theta})]\epsilon^*\}, \quad (18g)$$

$$m_{i,i+1} = 1, \quad (18h)$$

$$m_{ij} = 0, \quad 1 < j < i, \quad j \geq i + 2. \quad (18i)$$

The stability condition requires that the real part of all the eigenvalues  $\gamma$  of the matrix  $M$  is nonnegative.<sup>1</sup>

<sup>1</sup> In the following the operation  $\gamma \rightarrow \Re(\gamma)$  is understood.

The sign for the stability depends on the convention set by Eq. (7); nonpositive eigenvalues correspond to fixed points that are stable in the past.

For the dS fixed points, the Jordan equation  $\det(M - \gamma) = 0$  is simply

$$\gamma^2 \left( \frac{\sigma^*}{2} - \gamma \right) \cdots \left[ \frac{(\ell - 1)\sigma^*}{2} - \gamma \right] = 0, \quad (19)$$

and stability is guaranteed for  $\sigma^* > 0$  (blue-tilted spectra).

The power-law case is more complicated since one cannot easily diagonalize the matrix. The only notable exception is the Gauss–Bonnet braneworld with a normal scalar field. In that case,  $\lambda_\ell^* = 0$  for  $\ell \geq 2$  and the eigenvalue equation reads

$$(\gamma^2 - 2\epsilon^{*2}) \left( \frac{\epsilon^*}{2} - \gamma \right) \cdots \left[ \frac{(\ell - 1)\epsilon^*}{2} - \gamma \right] = 0. \quad (20)$$

The first two eigenvalues are equal in absolute value and opposite in sign. Therefore the power-law fixed points in GB  $\phi$ -inflation are a repeller in both backward and forward integration.

In other cases of interest a full analysis is required; moreover, one should check the stability in both backward and forward time integration and along a “sufficient” number of directions in the parameter space. If all the eigenvalues have the same sign, then there is an attractor either in the past or in the future. Conversely, if some of them have relative opposite sign, there is no attractor. The truncation order is also important, since higher-order terms can change the sign of the eigenvalues.

To determine the minimum level at which the stability analysis is reliable, we have solved the Jordan equation at the power-law fixed points from first order ( $2 \times 2$  matrix) to 10<sup>th</sup> order in the flow parameters ( $\ell = 10$ ), and checked that the real parts of the eigenvalues have different signs at higher orders. Figure 1 shows the eigenvalues of the 4D and RS models with a normal scalar field and the GB tachyon case. The GB  $\phi$  case is as described above, while the other tachyon plots are quite similar to that presented here.

Qualitatively these results do not depend on the actual value of  $\epsilon^*$ ; the only assumption is  $\epsilon^* > 0$ . As regards the level of approximation, for the normal scalar field and the 4D tachyon the first order is already sufficient to give the result holding at all higher orders, while in the RS and GB tachyon cases all eigenvalues are negative up to 2<sup>nd</sup> and 3<sup>rd</sup> order, respectively. At higher orders one eigenvalue becomes and remains positive. Note that the degeneracy of one of the eigenvalues (the lowest one in the RS  $\phi$  and GB  $T$  cases) is lifted every two orders (at even orders in the cited example).

The integration of the flow equations, performed at 5<sup>th</sup> order (see below), confirms these results. Therefore one can conclude that the power-law fixed points are unstable in both time directions, for all the present cosmological models, and at any (high) order in the flow truncation.

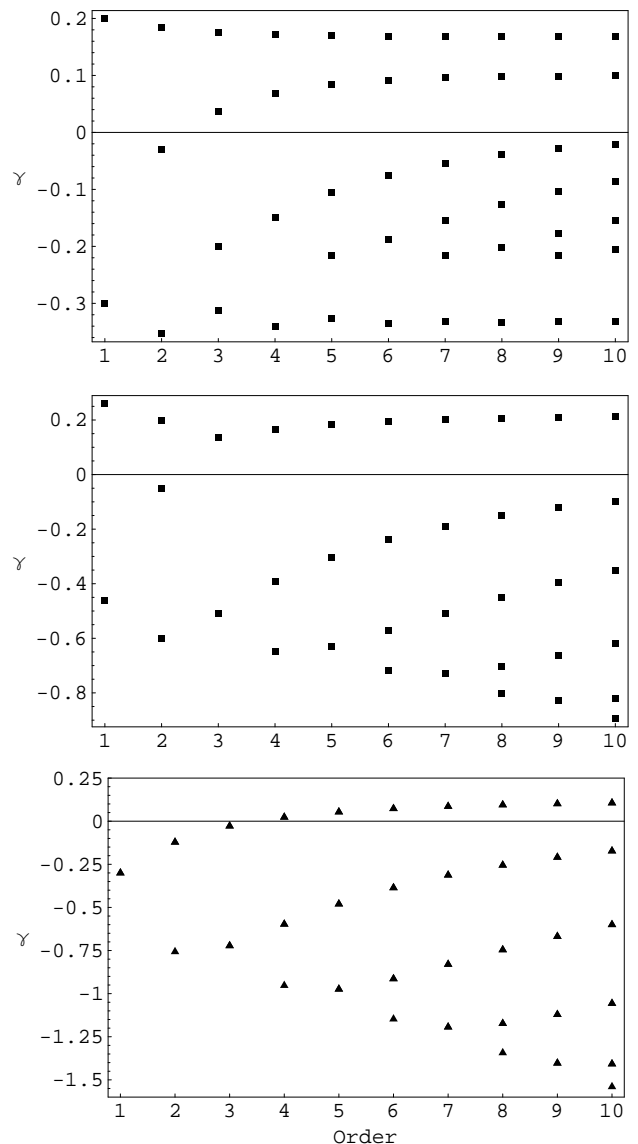


FIG. 1: Real part of the eigenvalues of the perturbation matrix for power-law fixed points, from 1<sup>st</sup> to 10<sup>th</sup> order in the flow parameters. From top to bottom, the 4D  $\phi$ , RS  $\phi$ , and GB  $T$  models are shown for  $\epsilon^* = 0.1$ .

The latter has been shown to be consistent in all cases from 4<sup>th</sup> order on.

### III. NUMERICAL INTEGRATION OF THE FLOW EQUATIONS

In order to study the evolution of the flow parameters, we have to establish a truncation level for the flow hierarchy and set suitable ranges of initial conditions for the parameters themselves within which they are randomly selected. Early flow papers solved the flow hierarchy numerically [6], but a more efficient approach [14] exploits an analytic solution to the flow equations found

in Ref. [7]:

$$H(\psi) = H_0 \left[ 1 + \sum_{\ell=1}^{M+1} A_\ell \psi^\ell \right], \quad (21)$$

where  $H_0 = H(t_0)$  is evaluated at the initial integration time  $t_0$ ; without loss of generality we choose  $\psi(t_0) = 0$ . This solution continues to be valid in all cases considered here. With the above normalization for the scalar field the coefficients  $A_\ell$  are dimensionless:

$$A_\ell = \frac{(-1)^\ell \lambda_{\ell-1}}{\ell! \epsilon^{(\ell-2)/2}} \Big|_{\psi=0}, \quad \ell \geq 1, \quad (22)$$

where  $\lambda_{\ell-1=0} = 1$ . The choice of the  $-$  sign, coming from the  $(H')^{\ell-1}$  term in Eq. (9b), is a convention determined by the rolling direction of the scalar field, which in this case is such that  $\dot{\psi} > 0$ :

$$-\frac{H'}{H} = \left( \frac{H}{H_0} \right)^{\tilde{\theta}/2} \sqrt{\epsilon}. \quad (23)$$

Note the coefficients Eq. (22) have a different normalization with respect to Ref. [14], due to dimensionless factors such as  $\sqrt{4\pi}$  absorbed into the definition of  $\psi$ .

To obtain the full evolution of the flow parameters, one needs only numerically integrate the relation between  $N$  and  $\psi$ , which from Eq. (8) is

$$dN = -\sqrt{\frac{1}{\epsilon} \left( \frac{H}{H_0} \right)^{\tilde{\theta}}} d\psi. \quad (24)$$

For each model we used the same sequence of 40,000 initial conditions chosen within the ranges [6]

$$\begin{aligned} \epsilon_0 &= [0, 0.8], \\ \sigma_0 &= [-0.5, 0.5], \\ \lambda_{2,0} &= [-0.05, 0.05], \\ \lambda_{3,0} &= [-0.005, 0.005], \\ &\dots \\ \lambda_{6,0} &= 0. \end{aligned} \quad (25)$$

For an implementation at 5<sup>th</sup> order in slow-roll the value of the last parameter truncates the series and closes the hierarchy. Initial conditions which do not generate either a sufficient amount of inflation or a well-defined asymptotic behaviour are rejected. Conversely, when enough inflation is realized, then either

1. The evolution proceeds until the end of inflation,  $\epsilon(t_f) = 1$ . Then the flow equations are integrated backwards for a suitable number of  $e$ -foldings where the observables  $n_s$  and  $r$  are evaluated and plotted, or
2. A late-time attractor is reached and the observables are read off at that point.

TABLE I: Population counts of forward integrated, backward integrated, and attractor points in the plots of Fig. 2, as percentages of a set of 40,000 entries.

	%	$N_0 \geq 50$	$N_0 < 50$	Attractor
$\phi$	4D	0.2	6.8	93.0
	RS	0.1	4.5	95.4
	GB	0.5	16.7	82.8
$T$	4D	0.1	4.6	95.3
	RS	0.1	3.9	96.0
	GB	0.1	5.7	94.2

The reference number of  $e$ -folds for the backward/forward integration can be either fixed or randomly chosen within a range. Here we take  $N_0 = 50$ , although the results will not depend significantly upon its precise value [6]. Also, we can distinguish points evolving to  $\epsilon_f = 1$  in two subcases:

- 1a. More than 50  $e$ -foldings of inflation are obtained from the initial point, meaning that the location where the observables are read off was reached by forwards integration from the initial condition.
- 1b. Less than 50  $e$ -foldings are obtained from the initial point, so that the point corresponding to the observables is obtained by integrating backwards in time from the initial condition.

The following results were all obtained via the approach described above. Additionally we checked that integrating the full flow hierarchy gives the same results point-by-point, which is a useful cross-check of the numerical implementation.

## IV. RESULTS

We divide our results into the (standard) commutative case and the noncommutative case. In the latter the flow equation evolution is unchanged, but the expression for the spectral index Eq. (16) is altered.

### A. The commutative case

Figure 2 shows the flow points in the  $n_s$ - $r$  plane for an ordinary and a tachyonic scalar field in the 4D, RS, and GB scenarios. The classification of points is model dependent and summarized in Table I. In all cases the attractor points are the dominant class, and hence the blue-tilted region ( $n_s > 1$ ) is more populated than the red-tilted one.

The points that finish inflation with 50  $e$ -foldings or more integrating forwards in time are a very small group of the three considered categories. Most of the points that finish inflation do so with less than 50  $e$ -foldings.

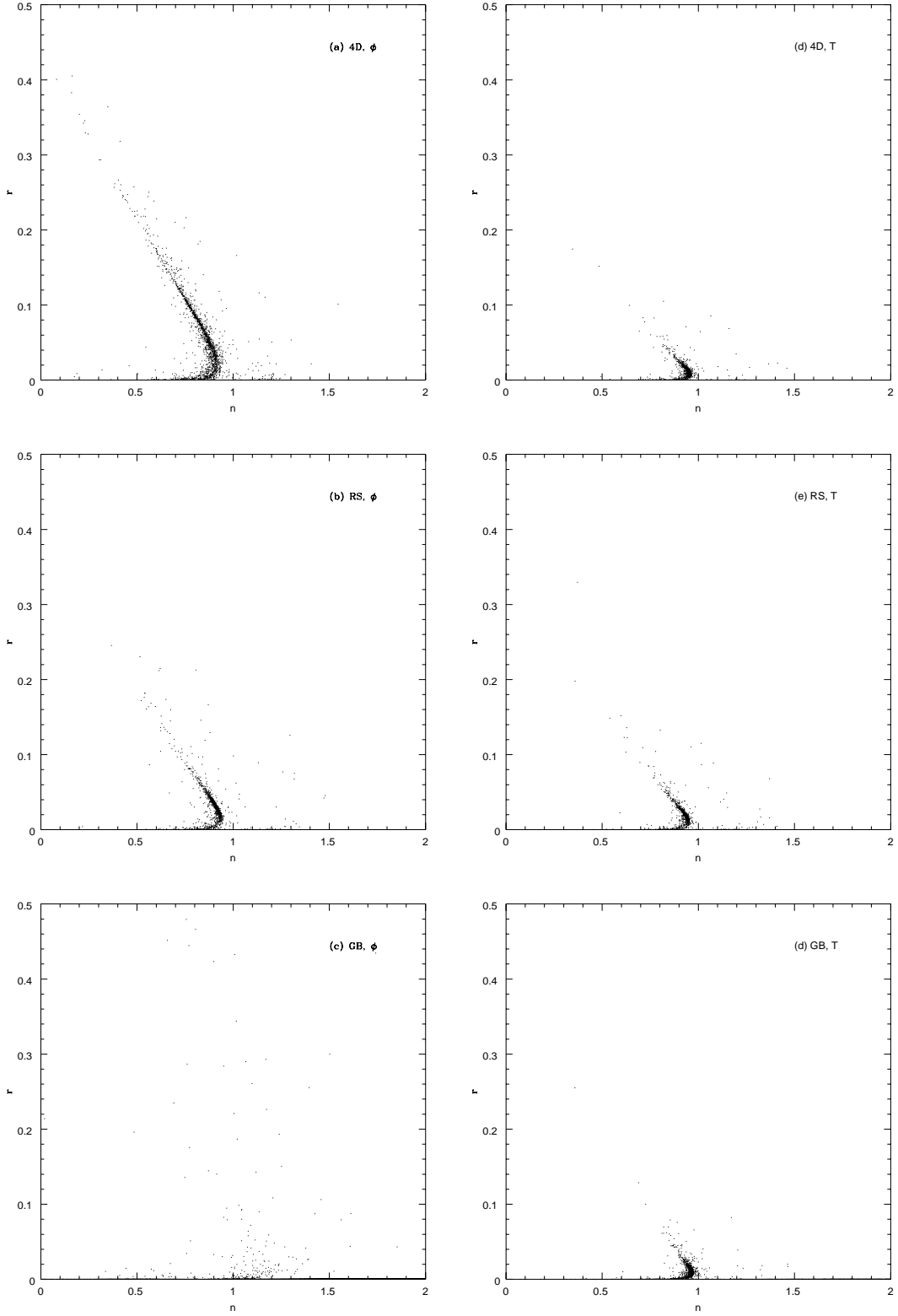


FIG. 2: Distribution of commutative inflationary observables in the  $n_s$ - $r$  plane. Left column: plots for an ordinary scalar field  $\phi$  in the a) 4D, b) RS, and c) GB cases. Right column: plots for a DBI scalar field  $T$  in the d) 4D, e) RS, and f) GB cases.

Note that what one does with the integration backwards is to find the point in parameter space where the initial condition should have been in order to give 50  $e$ -foldings or more. This does not necessarily correspond to the process that gave rise to the physical initial conditions for inflation to start.

Figure 2 roughly shows that the swathe near the power-law attractor decreases for increasing  $\theta$ , so that its vertical extension decreases from GB to 4D to RS. This is clear from Eq. (11a), since the second positive term in square brackets becomes more and more important. This seems to indicate faster flow, which would naturally give less height to the swathe as the natural flow is towards the  $r = 0$  line. Note that the swathe corresponds to the flow being integrated backwards in time from the initial point in order to generate 50  $e$ -foldings.

Comparing the percentages, it is clear that in the GB  $\phi$  case there is an increasing number of backward integrated points, eating off about 10% of the population of attractor points. Despite this fact, the swathe loses coherence and points spread in a large region in the observable plane, making the above descriptions rather approximate. Although there is no particular feature in the GB power-law attractor, the plot points do not lie close to it as in the other cases. This feature is a direct consequence of the flow equations. Equation (11) shows that the relevant parameter governing the cosmological evolution is  $\theta$  rather than  $q$ ; then the GB flow ( $\theta = -1$ ) would act in the opposite direction with respect to the RS ( $\theta = 1$ ) case, the 4D one being intermediate between the two. More precisely, while in RS the points are more concentrated at the region around  $r = 0$ ,  $n_s = 1$ , it is natural to expect more a widespread point distribution for GB. This does not necessarily imply that the GB braneworld is more severely constrained than the RS one.

In the GB  $\phi$  system, contrary to what happens in the others, all equations can be written in terms of  $\lambda_2$  and integrals of it. Since

$$\lambda_2 = \frac{d\lambda_1}{dN} + (1 + \tilde{\theta})\epsilon\lambda_1, \quad (26)$$

for  $\theta = \tilde{\theta} = -1 = -\bar{\theta}$  one has

$$\lambda_1 = \int \lambda_2 dN, \quad (27)$$

$$\lambda_\ell = \int [\lambda_{\ell+1} + (\ell - 1)\lambda_1\lambda_\ell] dN, \quad \ell \geq 2. \quad (28)$$

This property makes the numerical integration of the GB equation peculiar relative to the other models. Also, as shown in Sec. II C, the extra directions orthogonal to the  $n_s - r$  plane completely decouple in the dS and power-law cases ( $\lambda_\ell^* = 0$  for  $\ell \geq 2$ ). Therefore the two-dimensional analysis presented above is expected to encode all the relevant dynamical features.

In the tachyon case, the percentages do not change appreciably in different braneworlds, nor with respect to the ordinary scalar situation. This is because Eq. (8) is

insensitive to the type of braneworld in the tachyon case and the information on the extra dimension is carried only by the parameter  $\lambda_1$ . Therefore the tachyon plots are very similar to one another.

Also, in this case plot points are squeezed towards the dS attractor and prefer lower values of  $r$ . In order to understand why, let us define  $\varrho_\psi^2 \equiv \sigma^2 + r^2$ ; the difference of the (squared) radii for a fixed braneworld  $\{\zeta_q, \theta\}$  is, from Eq. (10),

$$\Delta^2 \equiv \varrho_\phi^2 - \varrho_T^2 = (2 - \theta)[4\lambda_1 - (10 + 3\theta)\epsilon]\epsilon. \quad (29)$$

For a given input set  $\{\epsilon, \lambda_1, \dots\}$  of parameters,  $\Delta^2 > 0$  in any case of interest considered so far and for the main part of initial conditions, which explains why the tachyon points are concentrated near the scale-invariant origin of the  $\sigma - r$  plane, while  $\phi$  points are more widespread through the plane. We verified numerically that  $\Delta^2 < 0$  in less than 10% of the cases. A similar argument, with the SR parameters now depending on the scalar field, can be applied for the large-field model plots of Ref. [15].

Note that these results are completely determined by the choice of the patch parameter  $\tilde{\theta}$ . The parameter  $\zeta_q$  would need to be extracted from the two-point correlation function of the graviton zero-mode within the original gravitational theory (3-brane in Einstein or Gauss-Bonnet gravity). However, one can redraw the plots in terms of the quantity  $\zeta_q r = O(r)$ , which differs from  $r$  only in the RS scenario. In this case, the only effect is a further squeezing (by a factor 2/3) of those points towards the dS attractor.

## B. The noncommutative case

Beside extra dimensions, one can take into account a modification of the space-time geometry at the quantum level. In particular, a space-time uncertainty principle is believed to be a universal property of high-energy theories motivated by strings [16]. This can be realized by a noncommutative algebra which preserves homogeneity and isotropy in the cosmological context [9]:

$$[\tau, x] = il_s^2, \quad (30)$$

where  $\tau \equiv \int a dt$  is a redefinition of time,  $x$  is a spatial coordinate on the brane, and  $l_s$  is the fundamental string length. In the simplest version of this model, moduli fields are fixed so that the extra dimension commutes with all the other directions.

The presence of a particular scale further breaks scale invariance and the perturbation spectra are affected accordingly. The detailed consequences of this ansatz were explored elsewhere [4, 15, 17]. Here we just recall that at large scales (corresponding to the strongly noncommutative limit) there are basically two different implementations for noncommutativity (“class 1” and “class 2”), depending on whether the Friedmann–Robertson–Walker 2-sphere is factored out from the measure of the action

for the cosmological perturbations or not. In both cases the background, flow equations, percentage populations of Table I, and stability analysis are not modified, and the new ingredient is encoded only in the expression for the scalar spectral index:

$$n_s - 1 \approx \sigma + c\epsilon, \quad (31)$$

where  $\sigma$  is defined in Eq. (10) and the constant  $c$  is  $c = 0$  in the commutative case,  $c = 2$  in the class 2 noncommutative model, and  $c = 6$  in the class 1 model. Since the scalar and tensor amplitudes are multiplied by a same extra factor depending on  $l_s$ , their ratio  $r$  is unchanged. Therefore the points in the upper region of the  $n_s$ - $r$  plane are shifted towards the right (blue-tilted spectra), while those lying on the  $r = 0$  line are unaffected. As one can see in Fig. 3, for  $c = 6$  the swathes point sharply rightwards instead of leftwards as in the commutative case. For  $c = 2$  the swathes are almost vertical. Thus the effect of noncommutativity is a skewing in the plane whose magnitude depends on the value of the parameter  $c$  [15].

Note that since the noncommutative correction to the spectral index is positive, the stability condition for the dS fixed points is again satisfied for blue-tilted spectra.

For brevity we have not shown tachyon plots in the noncommutative case, but their shape can readily be pictured by applying the same skewing to the points shown in Fig. 2.

### C. Relation to observations

We conclude by comparing the above flow plots with observations, with an analysis similar to that of Peiris *et al.* [2] and Makarov [11] for the standard cosmology. Present observations are highly restrictive in the  $n_s$ - $r$  plane, with only a small region near the origin still allowed in the plots we showed (very roughly, the allowed region corresponds to  $r < 0.03$  and  $0.95 < n_s < 1.1$ , but one must allow for those parameters being correlated). The regions where our plots show major differences are thus already excluded. We take the 95% likelihood bound of Ref. [18], conservatively choosing the wider region obtained without including Ly $\alpha$ -forest data, and compute in each case the fraction of points lying within that region (which we approximate by a suitably-oriented ellipse, noting that their  $r$  is defined to be 16 times ours). We do not impose a constraint from the spectral index running.

The percentage of points inside the allowed region is shown in Table II. In all cases the percentages are quite small, indicating that observations have already chopped off a substantial part of inflationary model space. Bearing in mind that the majority of the points are late-time attractor points with  $n_s > 1$  and negligible  $r$ , the strong constraint  $n_s < 1.04$  at  $r = 0$  [18] plays a major role in ensuring the percentages are so small. If this limit were further strengthened in the future to exclude blue-tilted models, all those points would be lost.

TABLE II: The percentage of points lying within the currently-allowed region for each of our cosmologies.

%		Commutative	Noncommutative	
			$c = 6$	$c = 2$
$\phi$	4D	0.1	0.6	0.3
	RS	0.1	1.9	0.3
	GB	0.4	0.3	0.3
$T$	4D	1.8	0.6	3.1
	RS	0.2	0.6	1.1
	GB	3.5	0.3	4.2

There are a couple of trends evident in the numbers. Firstly, the tachyon cases tend to give higher percentages, due to their suppression of the tensor ratio  $r$ . Secondly, for the normal scalar field, increasing the noncommutativity parameter  $c$  increases the percentages as it skews the swathes across to where the observations lie. Nevertheless, every cosmology proves capable of generating models within the allowed region, which prevents any useful conclusions from being drawn.

## V. CONCLUSIONS

In this paper we have analyzed braneworld and tachyon scenarios in terms of the flow evolution equations. The equations of motion and the stability of the associated fixed points have been considered in detail in the general relativistic, Randall–Sundrum, and Gauss–Bonnet cases at high order in the flow parameters. Each model generates different predictions for the main cosmological observables (scalar spectral index  $n_s$  and tensor-to-scalar ratio  $r$ ). In particular, Gauss–Bonnet gravity deeply modifies the flow structure in the parameter space for an ordinary inflaton field. In the cosmological tachyon case, the theoretical points in the  $n_s$ - $r$  plane are pressed towards scale invariance but the characteristic flow swathe does not lose coherence. We also discussed the imprint of a noncommutative geometry on the inflationary observables.

Some trends remain to be explored. In the braneworld inflationary scenarios the Weyl tensor is negligible at large scales and we have consistently neglected its contribution to the observables  $r$  and  $n_s$ . However, at small scales it can play an important role, as well as in the determination of other observables such as the bispectrum even at long wavelengths. Although we expect the flow approach to be unmodified by bulk physics, further investigation might clarify this point.

The flow equations approach is only one possible way in which one can generate an ensemble of inflationary models, corresponding to a Taylor expansion of  $H(\psi)$ . In Ref. [14], other methods were implemented in the general relativistic case to study the robustness of the flow equations structure, showing that there are significant

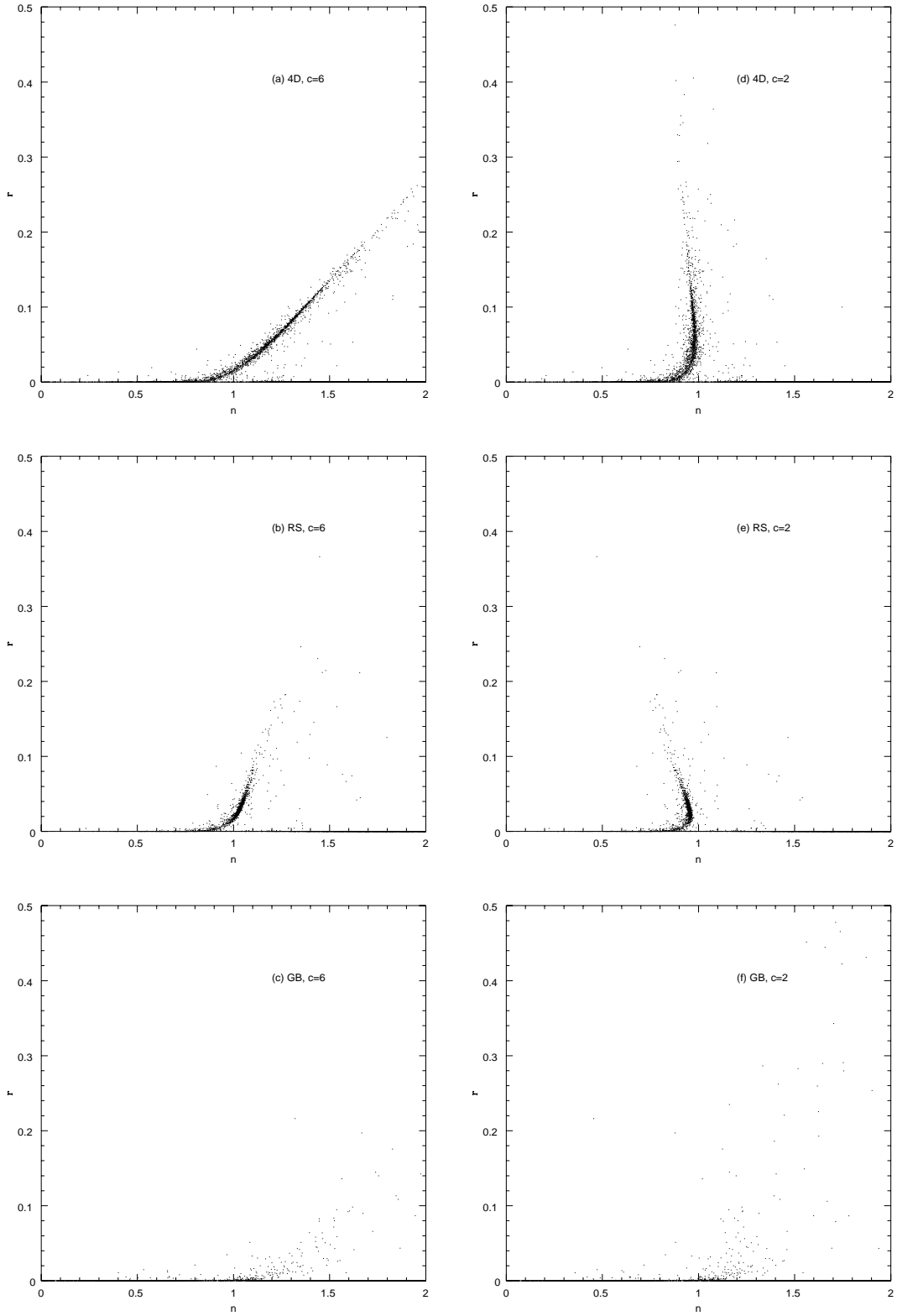


FIG. 3: Distribution of noncommutative inflationary observables in the  $n_s$ - $r$  plane for an ordinary scalar field  $\phi$ . Left column: plots for the class 1 model  $c = 6$  in the a) 4D, b) RS, and c) GB cases. Right column: plots for the class 2 model  $c = 2$  in the d) 4D, e) RS, and f) GB cases.

variations in outcome between methods. It may be interesting to explore these differences in the braneworld and tachyon cases, too.

### Acknowledgments

The work of G.C. is supported by JSPS, A.R.L. by PPARC, and E.R. by Conacyst.

- 
- [1] C. L. Bennett *et al.*, *Astrophys. J. Suppl.* **148**, 1 (2003) [astro-ph/0302207]; D. N. Spergel *et al.*, *Astrophys. J. Suppl.* **148**, 175 (2003) [astro-ph/0302209].
  - [2] H. V. Peiris *et al.*, *Astrophys. J. Suppl.* **148**, 213 (2003) [astro-ph/0302225].
  - [3] V. A. Rubakov, *Phys. Usp.* **44**, 871 (2001) [hep-ph/0104152]; R. Maartens, *Living Rev. Relativity* **7**, 7 (2004) [gr-qc/0312059]; P. Brax, C. van de Bruck, and A.-C. Davis, *Rept. Prog. Phys.* **67**, 2183 (2004) [hep-th/0404011]; C. Csáki, hep-ph/0404096.
  - [4] G. Calcagni, PhD thesis [hep-ph/0503044].
  - [5] M. B. Hoffman and M. S. Turner, *Phys. Rev. D* **64**, 023506 (2001) [astro-ph/0006321].
  - [6] W. H. Kinney, *Phys. Rev. D* **66**, 083508 (2002) [astro-ph/0206032].
  - [7] A. R. Liddle, *Phys. Rev. D* **68**, 103504 (2003) [astro-ph/0307286].
  - [8] E. Ramírez and A. R. Liddle, *Phys. Rev. D* **71**, 027303 (2005) [astro-ph/0412556].
  - [9] R. Brandenberger and P.-M. Ho, *Phys. Rev. D* **66**, 023517 (2002) [hep-th/0203119].
  - [10] A. R. Liddle, P. Parsons, and J. D. Barrow, *Phys. Rev. D* **50**, 7222 (1994) [astro-ph/9408015].
  - [11] A. Makarov, astro-ph/0506326.
  - [12] J.-F. Dufaux, J. E. Lidsey, R. Maartens, and M. Sami, *Phys. Rev. D* **70**, 083525 (2004) [hep-th/0404161].
  - [13] D. Langlois, R. Maartens, and D. Wands, *Phys. Lett. B* **489**, 259 (2000) [hep-th/0006007].
  - [14] E. Ramírez and A. R. Liddle, *Phys. Rev. D* **71**, 123510 (2005) [astro-ph/0502361].
  - [15] G. Calcagni and S. Tsujikawa, *Phys. Rev. D* **70**, 103514 (2004) [astro-ph/0407543].
  - [16] T. Yoneya, in *Wandering in the Fields*, edited by K. Kawarabayashi and A. Ukawa (World Scientific, Singapore, 1987), p. 419; M. Li and T. Yoneya, *Phys. Rev. Lett.* **78**, 1219 (1997) [hep-th/9611072]; T. Yoneya, *Prog. Theor. Phys.* **103**, 1081 (2000) [hep-th/0004074].
  - [17] Q.-G. Huang and M. Li, *J. High Energy Phys.* **06** (2003) 014 [hep-th/0304203]; S. Tsujikawa, R. Maartens, and R. Brandenberger, *Phys. Lett. B* **574**, 141 (2003) [astro-ph/0308169]; Q.-G. Huang and M. Li, *J. Cosmol. Astropart. Phys.* **11** (2003) 001 [astro-ph/0308458]; Q.-G. Huang and M. Li, *Nucl. Phys. B* **713**, 219 (2005) [astro-ph/0311378]; D. Liu and X. Li, *Phys. Rev. D* **70**, 123504 (2004) [astro-ph/0402063]; H. Kim, G. S. Lee, and Y. S. Myung, *Mod. Phys. Lett. A* **20**, 271 (2005) [hep-th/0402018]; H. Kim, G. S. Lee, H. W. Lee, and Y. S. Myung, *Phys. Rev. D* **70**, 043521 (2004) [hep-th/0402198]; R.-G. Cai, *Phys. Lett. B* **593**, 1 (2004) [hep-th/0403134]; Y. S. Myung, *Phys. Lett. B* **601**, 1 (2004) [hep-th/0407066]; D. Liu and X. Li, *Phys. Lett. B* **600**, 1 (2004) [hep-th/0409075]; K. Bamba and J. Yokoyama, *Phys. Rev. D* **70**, 083508 (2004) [hep-ph/0409237].
  - [18] U. Seljak *et al.*, astro-ph/0407372.